ARTICLE IN PRESS

Discrete Applied Mathematics ▮ (▮▮▮▮) ▮▮▮–▮▮▮

Contents lists available at ScienceDirect

Discrete Applied Mathematics

journal homepage: www.elsevier.com/locate/dam

Quality bounds for binary tomography with arbitrary projection matrices

W. Fortes [a,b], K.J. Batenburg [a,b,c,*]

[a] Centrum Wiskunde & Informatica, Science Park 123, 1098 XG Amsterdam, The Netherlands
[b] Mathematical Institute, Leiden University, The Netherlands
[c] iMinds-Vision Lab, University of Antwerp, Belgium

ARTICLE INFO

Article history:
Received 9 June 2013
Received in revised form 1 December 2013
Accepted 28 January 2014
Available online xxxx

Keywords:
Discrete tomography
Binary tomography
Error bounds
Underdetermined linear systems

ABSTRACT

Binary tomography deals with the problem of reconstructing a binary image from a set of its projections. The problem of finding binary solutions of underdetermined linear systems is, in general, very difficult and many such solutions may exist. In a previous paper we developed error bounds on differences between solutions of binary tomography problems restricted to projection models where the corresponding matrix has constant column sums. In this paper, we present a series of computable bounds that can be used with any projection model. In fact, the study presented here is not restricted to tomography and works for more general linear systems.

We report the results of computational experiments for some phantom images, focused on parallel and fan beam projection models. Our results show that in some cases the computed bounds can be used to prove that the difference between binary solutions must be small, even if the corresponding linear system is severely underdetermined.

1. Introduction

Binary tomography deals with the problem of reconstructing a binary image from its projections [11]. Projection images of an object are typically recorded using a scanning device, which employs a beam that is transmitted through the object (e.g. photons, electrons). An array of detectors records the beam intensity after the beam–object interaction, resulting in a projection of the object. Due to dose constraints or geometrical constraints on the angles for which projections can be acquired, the set of angles for which projections are acquired is often limited [9,13]. By exploiting the fact that the reconstructed image must be binary, it is often possible to compute useful reconstructions even if just a few projections are available [11]. However, such underdetermined binary tomography problems can have a large number of binary solutions, making it important to have a quality measure for the reconstruction with respect to the unknown original image.

The reconstruction problem can be modeled as a system of linear equations. The matrix that encodes these equations is known as the *projection matrix*. Depending on the particular type of tomography problem, different models can be used to define the projection matrix. In the *grid model*, which is a common model in *discrete tomography* [10,11], an image is formed by assigning a value to each point in a regular grid. In the *line model* and the *strip model*, one models a continuous image that is approximated on a grid of pixels having a constant gray value within each pixel. The results in this paper are restricted to

* Corresponding author at: Centrum Wiskunde & Informatica, Science Park 123, 1098 XG Amsterdam, The Netherlands. Tel.: +31 0 205924037; fax: +31 0 205924199.
E-mail addresses: wagner.fortes@cwi.nl (W. Fortes), joost.batenburg@cwi.nl, joost.batenburg@ua.ac.be (K.J. Batenburg).

http://dx.doi.org/10.1016/j.dam.2014.01.026
0166-218X/

Please cite this article in press as: W. Fortes, K.J. Batenburg, Quality bounds for binary tomography with arbitrary projection matrices, Discrete Applied Mathematics (2014), http://dx.doi.org/10.1016/j.dam.2014.01.026

binary tomography, but are not restricted to any particular projection model. The approach can be used for the grid model, but also for projection models used in continuous tomography, as will be further detailed in Section 7.1.

Our results are somewhat related to the stability problem in discrete tomography, which has been studied by several authors [1–3,8,15–17] for the grid model. The stability problem deals with the question whether a small perturbation of the observed data results in a small perturbation of the reconstruction. In our work, we deal with the problem how large the difference can be between binary solutions of a reconstruction problem, i.e. binary images that have *identical* projections.

Recently, quite general results were obtained allowing the computation of error bounds between images in binary tomography for any number of projection angles. In [18], a method is presented for computing bounds on the maximum distance between binary solution of tomography problems defined on a discrete grid. Related bounds for more general projection models are derived in [5]. Although in the latter article the tomography problem is presented in a general setting of a linear system of equations, the approach is limited to projection models for which the associated *projection matrix* has constant column sums (i.e. identical sums for all columns). The property of constant column sums holds in particular cases (e.g. the strip model for parallel beam tomography), but limits the application of the results to restricted cases (see Section 7.1 for projection models that do not satisfy this assumption). Although the bounds can still be approximated if this assumption is not completely satisfied, it is then no longer clear if they really provide a quality *guarantee*.

In this article, we derive error bounds that are more general than those in [5], as they can be applied to basically any problem modeled as an underdetermined algebraic linear system of equations. In particular, all relevant models of binary tomography fit within our generalized problem setting. Our generalization of the results from [5] is not at all automatic. New concepts and proofs are introduced to overcome the dependency on constant column sums, paving the way towards practical error bounds for binary tomography, which can be used, for example, when using a cone-beam projection model [20] or in the case of truncated projection data [19].

Although our focus is on tomography, our results are more general. We therefore consider the following general problem, of finding a binary vector that satisfies

$$\boldsymbol{A}\boldsymbol{x} = \boldsymbol{b}, \tag{1}$$

a consistent and underdetermined linear system of algebraic equations with $\boldsymbol{A} = (a_{ij}) \in \mathbb{R}^{m\times n}$, $m < n$, the vector of unknowns $\boldsymbol{x} = (x_j) \in \mathbb{R}^n$ and the right-hand side $\boldsymbol{b} = (b_i) \in \mathbb{R}^m$.

Finding a binary solution of Eq. (1) is often a very difficult problem and several binary solutions may exist. A given binary solution does not have to be close to another binary solution. In practice, the right hand side vector $\boldsymbol{b}$ is often obtained from an *original* binary vector $\boldsymbol{x}$ by a certain measurement procedure, modeled as the matrix $\boldsymbol{A}$. For a given measurement vector $\boldsymbol{b}$, it is unlikely that all binary solutions are representative solutions of the specific problem which yielded $\boldsymbol{b}$, since some solutions of Eq. (1) may be meaningless for physical problems. In such cases, it can be important to know how different these solutions can be. If one can give a bound on the maximum difference between two solutions, this also bounds the maximum difference between the *ground truth vector* (i.e., from which the vector of measured data $\boldsymbol{b}$ was obtained) and any other solution.

This article is structured as follows. In Section 2, we establish the notation which will be used throughout this article. In Section 3, different versions of bounds on the Euclidean norm of binary solutions are introduced. In Section 4, a general bound is derived on the difference between two binary solutions. Section 5 deals with bounds that are based on properties of the binary vectors that are obtained by rounding the minimum norm solution. These bounds are refined with a different approach in Section 6. Section 7 presents a series of simulation experiments for fan and parallel beam binary tomography and their results. From these results, the practical value of the proposed bounds can be evaluated for different kinds of problems. Section 8 concludes the article.

2. Notation and the minimum norm solution

For a given matrix $\boldsymbol{A}$ and given right-hand side $\boldsymbol{b}$, let $S_{\boldsymbol{A}}(\boldsymbol{b}) = \{\boldsymbol{x} \in \mathbb{R}^n : \boldsymbol{A}\boldsymbol{x} = \boldsymbol{b}\}$, the set of all real-valued solutions corresponding with the given data. A *binary vector* corresponds with a vector $\bar{\boldsymbol{x}} \in \{0, 1\}^n$. Let $\bar{S}_{\boldsymbol{A}}(\boldsymbol{b}) = S_{\boldsymbol{A}}(\boldsymbol{b}) \cap \{0, 1\}^n$, the set of *binary solutions* of the system.

Throughout this article, we use the vector $\mathbf{0}_t \in \mathbb{R}^t$ (for an integer $t > 0$), to denote a column vector consisting of t 0's, the vector $\mathbf{1}_t \in \mathbb{R}^t$ to denote a column vector consisting of t 1's and the identity matrix $\boldsymbol{I}_t \in \mathbb{R}^{t\times t}$. However, we often use the vectors $\mathbf{0}$ and $\mathbf{1}$ and the identity matrix $\boldsymbol{I}$ without specifying their dimension, as it does not compromise the understanding and clarity of the proofs.

For any two vectors $\bar{\boldsymbol{u}}, \bar{\boldsymbol{v}} \in \{0, 1\}^n$, define the *difference set* $\mathrm{D}(\bar{\boldsymbol{u}}, \bar{\boldsymbol{v}}) = \{i : \bar{u}_i \neq \bar{v}_i\}$ and the *number of differences* $\mathrm{d}(\bar{\boldsymbol{u}}, \bar{\boldsymbol{v}}) = \#\mathrm{D}(\bar{\boldsymbol{u}}, \bar{\boldsymbol{v}})$, where the symbol # denotes the cardinality operator for a finite set. Note that $\mathrm{d}(\bar{\boldsymbol{u}}, \bar{\boldsymbol{v}}) = \|\bar{\boldsymbol{u}} - \bar{\boldsymbol{v}}\|_1$.

For the following sections, consider the problem of finding a binary solution of a fixed linear system $\boldsymbol{A}\boldsymbol{x} = \boldsymbol{b}$ called the *binary solution problem*.

As the matrix $\boldsymbol{A}$ is not a square matrix, and may not have full rank, it does not have an inverse. Recall that the *Moore–Penrose pseudo-inverse* of an $m \times n$ matrix $\boldsymbol{A}$ is an $n \times m$ matrix $\boldsymbol{A}^\dagger$, which can be uniquely characterized by the two geometric conditions

$$\boldsymbol{A}^\dagger\boldsymbol{b} \perp \mathcal{N}(\boldsymbol{A}) \quad \text{and} \quad (\boldsymbol{I} - \boldsymbol{A}\boldsymbol{A}^\dagger)\boldsymbol{b} \perp \mathcal{C}(\boldsymbol{A}), \quad \forall \boldsymbol{b} \in \mathbb{R}^m,$$

where $\mathcal{N}(\boldsymbol{A})$ is the nullspace of $\boldsymbol{A}$ and $\mathcal{C}(\boldsymbol{A})$ is the *column space* of $\boldsymbol{A}$ [7, p. 15].

Please cite this article in press as: W. Fortes, K.J. Batenburg, Quality bounds for binary tomography with arbitrary projection matrices, Discrete Applied Mathematics (2014), http://dx.doi.org/10.1016/j.dam.2014.01.026

Let $\boldsymbol{x}^* = \boldsymbol{A}^\dagger \boldsymbol{b}$. Then $\boldsymbol{x}^*$ also has the property (see Chapter 3 of [6]) that it is a real-valued solution of minimal Euclidean norm of the system $\boldsymbol{Ax} = \boldsymbol{b}$, provided that such a solution exists. The minimum norm solution plays an important role in the bounds we will derive for the binary solution problem. Several methods are available for the computation of the minimum norm solutions. One approach is computing the QR decomposition of $\boldsymbol{A}^T$, see [4] for details. However, in several cases an iterative method, such as CGLS [14], is more suitable.

3. The Euclidean norm of binary solutions

The bounds on the difference between binary solutions that will be introduced in the upcoming sections are functions of the Euclidean norm of the solutions of the binary solution problem (1). In this section we present lower and upper bounds on the Euclidean norm (also referred to as *length*) of all binary solutions of the equation system (1).

If the matrix $\boldsymbol{A}$ has constant column sum k, the length of any binary solution can be determined directly from the data $\boldsymbol{b}$ [5]. Let $\bar{\boldsymbol{x}} \in \{0, 1\}^n$ and $\boldsymbol{b} = \boldsymbol{A}\bar{\boldsymbol{x}}$. Then

$$\sum_{i=1}^{m} b_i = \mathbf{1}_m^T \boldsymbol{b} = \mathbf{1}_m^T \boldsymbol{A}\bar{\boldsymbol{x}} = k\mathbf{1}_n^T \bar{\boldsymbol{x}} = k \sum_{j=1}^{n} \bar{x}_j$$

and hence $\|\bar{\boldsymbol{x}}\|_2^2 = \frac{\sum_{j=1}^{n} b_i}{k}$. This result also proves that if there is more than one binary vector satisfying $\boldsymbol{Ax} = \boldsymbol{b}$, all of them have the same length. However, if the matrix $\boldsymbol{A}$ does not have the property of constant column sums, the binary solutions of problem (1) may differ in length.

There are cases in which the matrix $\boldsymbol{A}$ almost has the property of constant column sums except for a very small discrepancy. It happens, for instance, due to numerical approximations. For such cases, there is a trivial way to obtain upper and lower bounds for the length of any binary solution, provided that a few conditions on $\boldsymbol{b}$ and $\boldsymbol{A}$ are satisfied:

Theorem 1. *Let* $\sum_{i=1}^{m} b_i \geq 0$, $\bar{\boldsymbol{x}} \in \bar{S}_{\boldsymbol{A}}(\boldsymbol{b})$ *and put* $\boldsymbol{v}^T = \mathbf{1}^T\boldsymbol{A}$. *Define* $\delta^+ = \max_{1\leq i\leq n} v_i$ *and* $\delta^- = \min_{1\leq i\leq n} v_i$, *the maximum and the minimum column sums of* $\boldsymbol{A}$, *respectively. Suppose that* $\delta^- > 0$. *Then* $\left\lceil \frac{\sum_{i=1}^{m} b_i}{\delta^+} \right\rceil \leq \|\bar{\boldsymbol{x}}\|_2^2 \leq \left\lfloor \frac{\sum_{i=1}^{m} b_i}{\delta^-} \right\rfloor$.

Proof.

$$\sum_{i=1}^{m} b_i = \mathbf{1}^T \boldsymbol{b} = \mathbf{1}^T \boldsymbol{A}\bar{\boldsymbol{x}} = \boldsymbol{v}^T \bar{\boldsymbol{x}} = \sum_{j=1}^{n} v_j \bar{x}_j, \tag{2}$$

and therefore

$$\frac{\sum_{i=1}^{m} b_i}{\delta^+} \leq \sum_{j=1}^{n} \bar{x}_j \leq \frac{\sum_{i=1}^{m} b_i}{\delta^-}. \tag{3}$$

As $\bar{\boldsymbol{x}} \in \{0, 1\}^n$, we have $\|\bar{\boldsymbol{x}}\|_2^2 = \|\bar{\boldsymbol{x}}\|_1 = \sum_{j=1}^{n} \bar{x}_j$ and

$$\left\lceil \frac{\sum_{i=1}^{m} b_i}{\delta^+} \right\rceil \leq \|\bar{\boldsymbol{x}}\|_2^2 \leq \left\lfloor \frac{\sum_{i=1}^{m} b_i}{\delta^-} \right\rfloor. \quad \square \tag{4}$$

However, if the difference $\left\lfloor \frac{\sum_{i=1}^{m} b_i}{\delta^-} \right\rfloor - \left\lceil \frac{\sum_{i=1}^{m} b_i}{\delta^+} \right\rceil$ is not very small, the bounds computed by Theorem 1 can be very different from the length of a binary solution $\bar{\boldsymbol{x}}$.

The bounds given in Theorem 1 are trivial to compute, but we note that better bounds can be obtained if the statement of the theorem is generalized to a linear programming (LP) formulation. In particular, for any $\boldsymbol{y} \in \boldsymbol{R}^m$ such that $\boldsymbol{y}^T\boldsymbol{A} \geq \mathbf{1}^T$, we have $\boldsymbol{y}^T\boldsymbol{A}\bar{\boldsymbol{x}} = \boldsymbol{y}^T\boldsymbol{b} \geq \mathbf{1}^T\bar{\boldsymbol{x}} = \|\bar{\boldsymbol{x}}\|_1$ (where the logical operator $\geq$ operates element-wise). Using linear programming to find the minimal such upper bound for which $\boldsymbol{y}^T\boldsymbol{A} \geq \mathbf{1}$ can provide a tighter bound on $\|\bar{\boldsymbol{x}}\|_1$ at the expense of significant computational cost. In tomography problems, $\boldsymbol{A}$ is typically very large (i.e. $> 10^4$ rows and columns), making linear programming a complex numerical problem, though it is theoretically tractable. In this paper, we aim to provide bounds that are relatively easy to compute, so we do not explore this direction further.

In the following theorems, we introduce more elaborate bounds on the length of any binary solution, which will be used in the remainder of this article. These bounds are computable by solving a linear system of equations (possibly iteratively) and do not require a linear programming algorithm.

Lemma 2. *Let* $\bar{\boldsymbol{x}} \in \bar{S}_{\boldsymbol{A}}(\boldsymbol{b})$, $\boldsymbol{x}^* = \boldsymbol{A}^\dagger\boldsymbol{b}$ *and* $\boldsymbol{e}^T = \mathbf{1}^T(\boldsymbol{I} - \boldsymbol{A}^\dagger\boldsymbol{A})$. *Then* $\|\bar{\boldsymbol{x}}\|_2^2 = \mathbf{1}^T\boldsymbol{x}^* + \boldsymbol{e}^T\bar{\boldsymbol{x}}$.

Please cite this article in press as: W. Fortes, K.J. Batenburg, Quality bounds for binary tomography with arbitrary projection matrices, Discrete Applied Mathematics (2014), http://dx.doi.org/10.1016/j.dam.2014.01.026

Proof. Let $\boldsymbol{y}_{LS}^T = \mathbf{1}^T\boldsymbol{A}^\dagger$ be the transpose of the minimum norm least squares solution of the linear system $\boldsymbol{A}^T\boldsymbol{y} = \mathbf{1}$. We have

$$\boldsymbol{A}^T\boldsymbol{y}_{LS} = \mathbf{1} - \boldsymbol{e},$$

with $\boldsymbol{e} = \mathbf{1} - \boldsymbol{A}^T\boldsymbol{y}_{LS} = (\boldsymbol{I} - \boldsymbol{A}^\dagger\boldsymbol{A})^T\mathbf{1}$, the residual. Note that in the case of constant column sums we have $\boldsymbol{e} = \mathbf{0}$, and this also holds in the more general case where $\mathbf{1}$ is in the row space of $\boldsymbol{A}$.

Left-multiplying the equality $\boldsymbol{A}\bar{\boldsymbol{x}} = \boldsymbol{b}$ by the vector $\boldsymbol{y}_{LS}^T$, we obtain

$$\boldsymbol{y}_{LS}^T\boldsymbol{A}\bar{\boldsymbol{x}} = (\mathbf{1}^T - \boldsymbol{e}^T)\bar{\boldsymbol{x}} = \boldsymbol{y}_{LS}^T\boldsymbol{b},$$

which yields

$$\begin{aligned}\mathbf{1}^T\bar{\boldsymbol{x}} &= \boldsymbol{y}_{LS}^T\boldsymbol{b} + \boldsymbol{e}^T\bar{\boldsymbol{x}}\\ &= \mathbf{1}^T\boldsymbol{x}^* + \boldsymbol{e}^T\bar{\boldsymbol{x}}.\end{aligned}$$

Since $\bar{\boldsymbol{x}} \in \{0, 1\}^n$, we have $\mathbf{1}^T\bar{\boldsymbol{x}} = \|\bar{\boldsymbol{x}}\|_1 = \|\bar{\boldsymbol{x}}\|_2^2$. □

Lemma 2 can be interpreted as follows: any solution of the underdetermined problem (1) can be written as the sum of a vector orthogonal to $\mathcal{N}(\boldsymbol{A})$ (i.e., the minimum norm solution) and the orthogonal projection of itself onto $\mathcal{N}(\boldsymbol{A})$. Hence, the sum of the elements of a solution is equal to the sum of the elements of the minimum norm solution plus the sum of the elements of the orthogonal projection of this solution onto the null space of $\boldsymbol{A}$. The orthogonal projector onto $\mathcal{N}(\boldsymbol{A})$ is given by $\boldsymbol{P} = (\boldsymbol{I} - \boldsymbol{A}^\dagger\boldsymbol{A})$.

Define $\boldsymbol{e}^T = \mathbf{1}^T(\boldsymbol{I} - \boldsymbol{A}^\dagger\boldsymbol{A})$, a *correction vector*, which will be frequently used throughout this article. Note that in Lemma 2 we focus on the vector $\boldsymbol{y}_{LS}$, whereas other vectors $\boldsymbol{y}$ could be used instead, possibly leading to tighter bounds. Similar to Theorem 1, our choice results in bounds that are straightforward to compute, whereas the introduction of an optimization approach could potentially yield improved bounds at the expense of computational complexity and cost.

Lemma 2 states that $\|\bar{\boldsymbol{x}}\|_2^2 = \mathbf{1}^T\boldsymbol{x}^* + \boldsymbol{e}^T\bar{\boldsymbol{x}}$, which cannot be computed exactly without knowing $\bar{\boldsymbol{x}}$. However, it is possible to bound $\|\bar{\boldsymbol{x}}\|_2^2$ as follows:

Theorem 3. *Let $\bar{\boldsymbol{x}} \in \bar{S}_{\boldsymbol{A}}(\boldsymbol{b})$ and $\boldsymbol{x}^* = \boldsymbol{A}^\dagger\boldsymbol{b}$. Then*

$$\left\lceil \mathbf{1}^T\boldsymbol{x}^* + \sum_{i\in\{j:e_j<0\}} e_i \right\rceil \le \|\bar{\boldsymbol{x}}\|_1 \le \left\lfloor \mathbf{1}^T\boldsymbol{x}^* + \sum_{i\in\{j:e_j>0\}} e_i \right\rfloor.$$

Proof. By Lemma 2, we have $\|\bar{\boldsymbol{x}}\|_2^2 = \mathbf{1}^T\boldsymbol{x}^* + \boldsymbol{e}^T\bar{\boldsymbol{x}}$, allowing $\|\bar{\boldsymbol{x}}\|_2^2$ to be bounded as

$$\mathbf{1}^T\boldsymbol{x}^* + \sum_{i=1}^{n} \min_{\bar{y}_i\in\{0,1\}} e_i\bar{y}_i \le \|\bar{\boldsymbol{x}}\|_2^2 \le \mathbf{1}^T\boldsymbol{x}^* + \sum_{i=1}^{n} \max_{\bar{y}_i\in\{0,1\}} e_i\bar{y}_i, \tag{5}$$

resulting in $\left\lceil \mathbf{1}^T\boldsymbol{x}^* + \sum_{i\in\{j:e_j<0\}} e_i \right\rceil \le \|\bar{\boldsymbol{x}}\|_2^2 \le \left\lfloor \mathbf{1}^T\boldsymbol{x}^* + \sum_{i\in\{j:e_j>0\}} e_i \right\rfloor$, as desired. □

The bounds given in Theorem 3 are based on the idea of implicitly selecting binary vectors to minimize or maximize the sum of the elements of the correction vector $\boldsymbol{e}$. However, this approach does not consider using the number of ones of these binary vectors to bound the length of the binary solutions.

Let ρ be a permutation of $\{1, \ldots, n\}$ such that $e_{\rho(1)} \ge e_{\rho(2)} \ge \cdots \ge e_{\rho(n)}$, which can be obtained by sorting the entries e_i in non-increasing order. We recall that e_i can also be negative.

Theorem 4. *Let $\bar{\boldsymbol{x}} \in \bar{S}_{\boldsymbol{A}}(\boldsymbol{b}) \setminus \{\mathbf{0}, \mathbf{1}\}$. Suppose that $\mathbf{1}^T\boldsymbol{x}^* + \boldsymbol{e}^T\mathbf{1} < n$. There is a unique $1 \le \ell < n$ such that*

(C1) $\ell + 1 > \mathbf{1}^T\boldsymbol{x}^* + \sum_{j=1}^{\ell+1} e_{\rho(j)}$ *and*

(C2) $\ell \le \mathbf{1}^T\boldsymbol{x}^* + \sum_{j=1}^{\ell} e_{\rho(j)}$.

For this ℓ, we have $\|\bar{\boldsymbol{x}}\|_1 = \|\bar{\boldsymbol{x}}\|_2^2 \le \ell$.

Proof. From Lemma 2, we have

$$\|\bar{\boldsymbol{x}}\|_1 = \mathbf{1}^T\boldsymbol{x}^* + \boldsymbol{e}^T\bar{\boldsymbol{x}} = \mathbf{1}^T\boldsymbol{x}^* + \sum_{i=1}^{n} e_i\bar{x}_i = \mathbf{1}^T\boldsymbol{x}^* + \sum_{i\in\{j:\bar{x}_j=1\}} e_i \le \mathbf{1}^T\boldsymbol{x}^* + \sum_{i=1}^{\|\bar{\boldsymbol{x}}\|_1} e_{\rho(i)}. \tag{6}$$

Please cite this article in press as: W. Fortes, K.J. Batenburg, Quality bounds for binary tomography with arbitrary projection matrices, Discrete Applied Mathematics (2014), http://dx.doi.org/10.1016/j.dam.2014.01.026

Consider the concave function $f(\ell) = \mathbf{1}^T\boldsymbol{x}^* + \sum_{i=1}^{\ell} e_{\rho(i)}$ and the function $g(\ell) = \ell$, for $\ell = 1, \ldots, n$. From Eq. (6), we know that $g(\|\bar{\boldsymbol{x}}\|_1) \leq f(\|\bar{\boldsymbol{x}}\|_1)$, and from the assumption of the Theorem, we have $f(n) = \mathbf{1}^T\boldsymbol{x}^* + \boldsymbol{e}^T\mathbf{1} < n = g(n)$.

As we want an upper bound for $\|\bar{\boldsymbol{x}}\|_1$, we now try to find the largest value of ℓ for which $g(\ell) \leq f(\ell)$. We distinguish the following cases:

1. $g(\ell) > f(\ell)$ for all $\ell = 1, \ldots, n$. Then there is no ℓ satisfying condition (C2), therefore this case cannot occur.
2. $g(\ell) \leq f(\ell)$ for $\ell = 1, \ldots, s$ and $g(\ell) > f(\ell)$ for $\ell = s+1, \ldots, n$. Then (C1) and (C2) are jointly satisfied only for $\ell = s$.
3. $g(\ell) > f(\ell)$ for $\ell = 1, \ldots, t-1$; $g(\ell) \leq f(\ell)$ for $\ell = t, \ldots, s$; $g(\ell) > f(\ell)$ for $\ell = s+1, \ldots, n$. Then (C1) and (C2) are jointly satisfied only for $\ell = s$.

If $g(\ell) < f(\ell)$ for all $\ell = 1, \ldots, n-1$, then $\mathbf{1}^T\boldsymbol{x}^* + \boldsymbol{e}^T\mathbf{1} \not< n$, which does not satisfy the assumptions of the Theorem. □

Example 5. Consider the linear system of equations $\boldsymbol{A}\boldsymbol{x} = \boldsymbol{b}$ with the set of binary solutions $\bar{S}_{\boldsymbol{A}}(\boldsymbol{b}) = \{\bar{\boldsymbol{x}}^{(1)}, \bar{\boldsymbol{x}}^{(2)}, \bar{\boldsymbol{x}}^{(3)}\}$ such that

$$\boldsymbol{A} = \begin{pmatrix} 1 & 1 & 0 & 1 & 0 \\ 0 & 1 & 1 & 0 & 1 \end{pmatrix}, \qquad \boldsymbol{b} = \begin{pmatrix} 2 \\ 1 \end{pmatrix}, \qquad \bar{\boldsymbol{x}}^{(1)} = \begin{pmatrix} 0 \\ 1 \\ 0 \\ 1 \\ 0 \end{pmatrix}, \qquad \bar{\boldsymbol{x}}^{(2)} = \begin{pmatrix} 1 \\ 1 \\ 0 \\ 0 \\ 0 \end{pmatrix} \quad \text{and} \quad \bar{\boldsymbol{x}}^{(3)} = \begin{pmatrix} 1 \\ 0 \\ 1 \\ 1 \\ 0 \end{pmatrix}.$$

In order to apply Theorem 4 and obtain an upper bound on the Euclidean norm of any binary solution of the given linear system, the correction vector $\boldsymbol{e} = (\boldsymbol{I} - \boldsymbol{A}^{\dagger}\boldsymbol{A})^T\mathbf{1}$ must be computed. The explicit computation of the pseudo-inverse $\boldsymbol{A}^{\dagger}$ is not necessary, as indicated in the proof of Lemma 2. Hence, we have $\boldsymbol{e}^T = \begin{pmatrix} 0.25 & -0.5 & 0.25 & 0.25 & 0.25 \end{pmatrix}$ and $\boldsymbol{x}^{*T} = \begin{pmatrix} 0.625 & 0.75 & 0.125 & 0.625 & 0.125 \end{pmatrix}$.

We check the conditions (C1) and (C2) of Theorem 4 for $0 \leq \ell < 5$, and find that they are satisfied only for $\ell = 3$:

$$4 > \mathbf{1}^T\boldsymbol{x}^* + \sum_{i=1}^{4} e_{\rho(i)} = 2.25 + 1 = 3.25 \quad \text{and} \quad 3 \leq \mathbf{1}^T\boldsymbol{x}^* + \sum_{i=1}^{3} e_{\rho(i)} = 2.25 + 0.75 = 3$$

which gives, for any $\bar{\boldsymbol{x}} \in \bar{S}_{\boldsymbol{W}}(\boldsymbol{p})$, $\|\bar{\boldsymbol{x}}\|_2^2 \leq 3$.

4. A bound based on the minimum norm solution

In this section, a first bound is derived on the distance between solutions of the binary reconstruction problem, which follows from the fact that the Euclidean distance between the minimum norm solution and any binary solution of Eq. (1) can be bounded by an expression based on the minimum norm solution and the elements of the correction vector. Similar bounds, but for a more restricted setting, are given in [18,5].

Lemma 6. *Let* $\bar{\boldsymbol{x}} \in \bar{S}_{\boldsymbol{A}}(\boldsymbol{b})$. *Then* $\|\bar{\boldsymbol{x}} - \boldsymbol{x}^*\|_2 = \sqrt{\|\bar{\boldsymbol{x}}\|_2^2 - \|\boldsymbol{x}^*\|_2^2}$.

Proof. From the definition of $\boldsymbol{x}^*$ we have $(\bar{\boldsymbol{x}} - \boldsymbol{x}^*) \in \mathcal{N}(\boldsymbol{A})$, and $\boldsymbol{x}^* \perp (\bar{\boldsymbol{x}} - \boldsymbol{x}^*)$. Applying Pythagoras' Theorem and Lemma 2 yields

$$\|\bar{\boldsymbol{x}} - \boldsymbol{x}^*\|_2^2 = \|\bar{\boldsymbol{x}}\|_2^2 - \|\boldsymbol{x}^*\|_2^2. \quad \square \tag{7}$$

For $\bar{\boldsymbol{x}} \in \bar{S}_{\boldsymbol{A}}(\boldsymbol{b})$, define $\mathcal{R}_{\boldsymbol{A},\boldsymbol{b}}(\bar{\boldsymbol{x}}) = \sqrt{\|\bar{\boldsymbol{x}}\|_2^2 - \|\boldsymbol{x}^*\|_2^2}$. We refer to $\mathcal{R}_{\boldsymbol{A},\boldsymbol{b}}(\bar{\boldsymbol{x}})$ as the *central radius of* $\bar{\boldsymbol{x}}$. According to Lemma 6, any binary solution $\bar{\boldsymbol{x}}$ of problem (1) is on the hypersphere centered in $\boldsymbol{x}^*$ with radius $\mathcal{R}_{\boldsymbol{A},\boldsymbol{b}}(\bar{\boldsymbol{x}})$. Notice that different binary solutions of problem (1) may lie on different hyperspheres.

Some of the results in the remainder of this article require a definition of the central radius that is also valid for $\bar{\boldsymbol{x}} \in \{0,1\}^n$ that are not in the solution set of $\boldsymbol{A}\boldsymbol{x} = \boldsymbol{b}$. We therefore introduce the more general definition $\mathcal{R}_{\boldsymbol{A},\boldsymbol{b}}(\bar{\boldsymbol{x}}) = \sqrt{\mathbf{1}^T\boldsymbol{x}^* + \boldsymbol{e}^T\bar{\boldsymbol{x}} - \|\boldsymbol{x}^*\|_2^2}$. Notice that if $\bar{\boldsymbol{x}} \in \bar{S}_{\boldsymbol{A}}(\boldsymbol{b})$, both definitions are equivalent.

In further theorems, we are interested in computing $R \in \mathbb{R}$ such that $R \geq \mathcal{R}_{\boldsymbol{A},\boldsymbol{b}}(\bar{\boldsymbol{x}})$ for all $\bar{\boldsymbol{x}} \in \bar{S}_{\boldsymbol{A}}(\boldsymbol{b})$, i.e, we want an upper bound for all $\mathcal{R}_{\boldsymbol{A},\boldsymbol{b}}(\bar{\boldsymbol{x}})$ with $\bar{\boldsymbol{x}} \in \bar{S}_{\boldsymbol{A}}(\boldsymbol{b})$. To this end, the bound R can be computed by Lemma 6 combined either with Theorems 1, 3 or 4. If we also consider the lower bound from Theorem 3 (or 1), we obtain two radii defining a spherical shell centered in $\boldsymbol{x}^*$ containing all binary solutions.

Supposing the existence of at least two different binary solutions, the upper bound R of the central radius allows us to derive an upper bound for the number of entry differences between those solutions.

Theorem 7. *Let* $\bar{\boldsymbol{x}}, \bar{\boldsymbol{y}} \in \bar{S}_{\boldsymbol{A}}(\boldsymbol{b})$ *and* $R \geq \mathcal{R}_{\boldsymbol{A},\boldsymbol{b}}(\bar{\boldsymbol{u}})$, *for all* $\bar{\boldsymbol{u}} \in \bar{S}_{\boldsymbol{A}}(\boldsymbol{b})$. *Then* $\mathrm{d}(\bar{\boldsymbol{x}}, \bar{\boldsymbol{y}}) \leq 4R^2$.

Please cite this article in press as: W. Fortes, K.J. Batenburg, Quality bounds for binary tomography with arbitrary projection matrices, Discrete Applied Mathematics (2014), http://dx.doi.org/10.1016/j.dam.2014.01.026

Proof. According to Lemma 6, we have $\|\bar{\boldsymbol{x}} - \boldsymbol{x}^*\|_2 = \mathcal{R}_{\boldsymbol{A},\boldsymbol{b}}(\bar{\boldsymbol{x}})$ and $\|\bar{\boldsymbol{y}} - \boldsymbol{x}^*\|_2 = \mathcal{R}_{\boldsymbol{A},\boldsymbol{b}}(\bar{\boldsymbol{y}})$. Therefore,

$$\|\bar{\boldsymbol{x}} - \bar{\boldsymbol{y}}\|_2 \leq \|\bar{\boldsymbol{x}} - \boldsymbol{x}^*\|_2 + \|\bar{\boldsymbol{y}} - \boldsymbol{x}^*\|_2 = \mathcal{R}_{\boldsymbol{A},\boldsymbol{b}}(\bar{\boldsymbol{x}}) + \mathcal{R}_{\boldsymbol{A},\boldsymbol{b}}(\bar{\boldsymbol{y}}) \leq 2R. \tag{8}$$

As $\bar{\boldsymbol{x}}$ and $\bar{\boldsymbol{y}}$ are binary, we have $\mathrm{d}(\bar{\boldsymbol{x}}, \bar{\boldsymbol{y}}) = \|\bar{\boldsymbol{x}} - \bar{\boldsymbol{y}}\|_1 = \|\bar{\boldsymbol{x}} - \bar{\boldsymbol{y}}\|_2^2$. □

5. Bounds based on rounding the minimum norm solution

In this section we repeat several results of [5] (without their proof), which can be extended to the case of non-constant column sums of the projection matrix, simply by using an upper bound on the central radius instead of using the exact central radius (as in [5]). In the experiments of Section 7, these bounds will be compared to the new bounds introduced in Section 6. The results of this section are expressed as theorems and are illustrated by an example.

The fact that the elements of $\bar{S}_{\boldsymbol{A}}(\boldsymbol{b})$ surround the minimum norm solution $\boldsymbol{x}^*$, suggests that binary solutions can often be found near $\boldsymbol{x}^*$. It is therefore natural to consider the vector that is obtained by rounding each entry of $\boldsymbol{x}^*$ to the nearest binary value. The following bounds are based on the number of differences between a binary solution of problem (1) and a binary vector obtained by rounding $\boldsymbol{x}^*$.

Let $\mathcal{T} = \{\bar{\boldsymbol{w}} \in \{0,1\}^n : \|\bar{\boldsymbol{w}} - \boldsymbol{x}^*\|_2 \leq \|\bar{\boldsymbol{u}} - \boldsymbol{x}^*\|_2, \text{ for all } \bar{\boldsymbol{u}} \in \{0,1\}^n\}$. Note that the elements of $\mathcal{T}$ correspond to the possible pixel-wise roundings of $\boldsymbol{x}^*$ to binary values. If none of the entries of $\boldsymbol{x}^*$ equals $\frac{1}{2}$, $\mathcal{T}$ contains a single element and the number of elements is doubled for each occurrence of $\frac{1}{2}$. Let $\bar{\boldsymbol{r}} \in \mathcal{T}$, i.e., $\bar{\boldsymbol{r}}$ is among the binary vectors that are nearest to $\boldsymbol{x}^*$ in the Euclidean sense. Put $T = \|\bar{\boldsymbol{r}} - \boldsymbol{x}^*\|_2$, i.e., the Euclidean distance from $\boldsymbol{x}^*$ to the nearest binary vector. If $R > T$ and $R - T$ is small, it is possible to say that a fraction of the rounded values are correct, i.e., to provide an upper bound on the *number* of entry differences between any solution in $\bar{S}_{\boldsymbol{A}}(\boldsymbol{b})$ and $\bar{\boldsymbol{r}}$. In most cases we cannot say *which* rounded values are correct.

For the next Lemma, recall that $\mathrm{D}(\bar{\boldsymbol{u}}, \bar{\boldsymbol{v}}) = \{i : \bar{u}_i \neq \bar{v}_i\}$.

Lemma 8. *Let $\bar{\boldsymbol{r}} \in \mathcal{T}$ and $\bar{\boldsymbol{x}} \in \bar{S}_{\boldsymbol{A}}(\boldsymbol{b})$. Then $\mathcal{R}^2_{\boldsymbol{A},\boldsymbol{b}}(\bar{\boldsymbol{x}}) - T^2 = \sum_{i \in \mathrm{D}(\bar{\boldsymbol{x}},\bar{\boldsymbol{r}})} |2x^*_i - 1|$.*

Define $\beta_i = |2x^*_i - 1|$ and let π be a permutation of $\{1, \ldots, n\}$ such that $\beta_{\pi(1)} \leq \beta_{\pi(2)} \leq \cdots \leq \beta_{\pi(n)}$, which can be obtained by sorting the entries β_i in increasing order.

Theorem 9. *Let $\bar{\boldsymbol{r}} \in \mathcal{T}$ and $R \geq \mathcal{R}_{\boldsymbol{A},\boldsymbol{b}}(\bar{\boldsymbol{u}})$, for all $\bar{\boldsymbol{u}} \in \bar{S}_{\boldsymbol{A}}(\boldsymbol{b})$. Put*

$$U = \max\left\{0 \leq \ell \leq n : \sum_{i=1}^{\ell} \beta_{\pi(i)} \leq R^2 - T^2\right\}.$$

Then for any $\bar{\boldsymbol{x}} \in \bar{S}_{\boldsymbol{A}}(\boldsymbol{b})$, we have $\mathrm{d}(\bar{\boldsymbol{r}}, \bar{\boldsymbol{x}}) \leq U$.

Theorem 9 is based in the following: consider the set of entries where $\bar{\boldsymbol{r}}$ and $\bar{\boldsymbol{x}}$ are different. If we transform $\bar{\boldsymbol{r}}$ into $\bar{\boldsymbol{x}}$ by performing a sequence of single-entry changes (either from 0 to 1, or from 1 to 0), each time an entry i of $\bar{\boldsymbol{r}}$ is changed the squared Euclidean distance from the current vector to $\boldsymbol{x}^*$ increases by $\beta_i = |2x^*_i - 1|$. As all binary solutions of problem (1) are on hyperspheres centered in $\boldsymbol{x}^*$ with radius smaller or equal than R (computed, e.g., by Theorem 4), we know that once we have crossed the boundary of the hypersphere with radius R, a binary solution can no longer be obtained by changing the values of additional entries that have not yet been changed. An upper bound on the number of differences between $\bar{\boldsymbol{r}}$ and $\bar{\boldsymbol{x}}$ can be obtained by counting the number of steps required to cross the hypersphere, each time choosing a pixel which results in the minimal increase in the relative distance to the boundary.

Example 10. Using the same data as given in Example 5, we compute

$$\boldsymbol{x}^* = \begin{pmatrix} 0.65 \\ 0.75 \\ 0.125 \\ 0.625 \\ 0.125 \end{pmatrix}, \quad \bar{\boldsymbol{r}} = \begin{pmatrix} 1 \\ 1 \\ 0 \\ 1 \\ 0 \end{pmatrix}, \quad \beta = \begin{pmatrix} 0.25 \\ 0.5 \\ 0.75 \\ 0.25 \\ 0.75 \end{pmatrix} \quad \text{and} \quad \beta_\pi = \begin{pmatrix} 0.25 \\ 0.25 \\ 0.5 \\ 0.75 \\ 0.75 \end{pmatrix},$$

where $\bar{\boldsymbol{r}}$ is obtained by rounding the entries of $\boldsymbol{x}^*$ to binary values. Then, we compute $T^2 = \|\bar{\boldsymbol{r}} - \boldsymbol{x}^*\|_2^2 = 0.375$ and, from Lemma 6 and Example 5, $R^2 = 1.625 \geq \|\bar{\boldsymbol{x}}\|_2^2 - \|\boldsymbol{x}^*\|_2^2$.

Applying Theorem 9, we verify, for $0 \leq \ell \leq 5$, that

$$\sum_{i=0}^{3} \beta_{\pi(i)} = 1 \leq 1.25 = R^2 - T^2 \quad \text{and} \quad \sum_{i=0}^{4} \beta_{\pi(i)} = 1.75 \not\leq 1.25 = R^2 - T^2.$$

Then for any $\bar{\boldsymbol{x}} \in \bar{S}_{\boldsymbol{A}}(\boldsymbol{b})$, we have $\mathrm{d}(\bar{\boldsymbol{r}}, \bar{\boldsymbol{x}}) \leq 3$.

Please cite this article in press as: W. Fortes, K.J. Batenburg, Quality bounds for binary tomography with arbitrary projection matrices, Discrete Applied Mathematics (2014), http://dx.doi.org/10.1016/j.dam.2014.01.026

Theorem 11. *Let $\bar{\boldsymbol{x}}, \bar{\boldsymbol{y}} \in \bar{S}_{\boldsymbol{A}}(\boldsymbol{b})$, $\bar{\boldsymbol{r}} \in \mathcal{T}$ and $R \geq \mathcal{R}_{\boldsymbol{A},\boldsymbol{b}}(\bar{\boldsymbol{u}})$, for all $\bar{\boldsymbol{u}} \in \bar{S}_{\boldsymbol{A}}(\boldsymbol{b})$. Put*

$$U = \max\left\{0 \leq \ell \leq n : \sum_{i=1}^{\ell} \beta_{\pi(i)} \leq 2\left(R^2 - T^2\right)\right\}.$$

Then $\mathrm{d}(\bar{\boldsymbol{x}}, \bar{\boldsymbol{y}}) \leq U$.

6. Bounds based on a subsequent radius reduction

In this section we do not use the upper bound for the length of binary solutions given by Theorems 1 or 4, but the one from Theorem 3 only. Recall from the proof of Theorem 3 that a binary vector $\bar{\boldsymbol{z}}$ can be constructed (not necessarily a solution of the binary solution problem), which maximizes the central radius, i.e., $\bar{\boldsymbol{z}} \in \{\bar{\boldsymbol{w}} \in \{0,1\}^n : \mathcal{R}_{\boldsymbol{A},\boldsymbol{b}}(\bar{\boldsymbol{w}}) \geq \mathcal{R}_{\boldsymbol{A},\boldsymbol{b}}(\bar{\boldsymbol{u}}),\ \text{for all } \bar{\boldsymbol{u}} \in \{0,1\}^n\}$. After computing the largest central radius $\mathcal{R}_{\boldsymbol{A},\boldsymbol{b}}(\bar{\boldsymbol{z}})$, a radius reduction is performed based on a function depending on the correction vector $\boldsymbol{e}$ and the binary vector $\bar{\boldsymbol{r}}$ closest to the minimum norm solution $\boldsymbol{x}^*$ (the center of the hypersphere containing all binary solutions). For the next theorems, recall that $\boldsymbol{e}^T = \mathbf{1}^T(\boldsymbol{I} - \boldsymbol{A}^{\dagger}\boldsymbol{A})$ and $T = \|\bar{\boldsymbol{r}} - \boldsymbol{x}^*\|_2$.

Lemma 12. *Let $\bar{\boldsymbol{x}}, \bar{\boldsymbol{y}} \in \{0,1\}^n$. Then, $\mathcal{R}^2_{\boldsymbol{A},\boldsymbol{b}}(\bar{\boldsymbol{x}}) = \mathcal{R}^2_{\boldsymbol{A},\boldsymbol{b}}(\bar{\boldsymbol{y}}) - \sum_{i=1}^n e_i(\bar{y}_i - \bar{x}_i)$.*

Proof. As $\mathcal{R}^2_{\boldsymbol{A},\boldsymbol{b}}(\bar{\boldsymbol{x}}) = \mathbf{1}^T\boldsymbol{x}^* + \boldsymbol{e}^T\bar{\boldsymbol{x}} - \|\boldsymbol{x}^*\|_2^2$ and $\mathcal{R}^2_{\boldsymbol{A},\boldsymbol{b}}(\bar{\boldsymbol{y}}) = \mathbf{1}^T\boldsymbol{x}^* + \boldsymbol{e}^T\bar{\boldsymbol{y}} - \|\boldsymbol{x}^*\|_2^2$, we have

$$\mathcal{R}^2_{\boldsymbol{A},\boldsymbol{b}}(\bar{\boldsymbol{y}}) - \mathcal{R}^2_{\boldsymbol{A},\boldsymbol{b}}(\bar{\boldsymbol{x}}) = \boldsymbol{e}^T(\bar{\boldsymbol{y}} - \bar{\boldsymbol{x}}).$$

Hence, $\mathcal{R}^2_{\boldsymbol{A},\boldsymbol{b}}(\bar{\boldsymbol{x}}) = \mathcal{R}^2_{\boldsymbol{A},\boldsymbol{b}}(\bar{\boldsymbol{y}}) - \sum_{i=1}^n e_i(\bar{y}_i - \bar{x}_i)$. □

Lemma 13. *Let $\bar{\boldsymbol{x}} \in \bar{S}_{\boldsymbol{A}}(\boldsymbol{b})$, $\bar{\boldsymbol{r}} \in \mathcal{T}$ and $\bar{\boldsymbol{z}} \in \{\bar{\boldsymbol{w}} \in \{0,1\}^n : \mathcal{R}_{\boldsymbol{A},\boldsymbol{b}}(\bar{\boldsymbol{w}}) \geq \mathcal{R}_{\boldsymbol{A},\boldsymbol{b}}(\bar{\boldsymbol{u}}),\ \text{for all } \bar{\boldsymbol{u}} \in \{0,1\}^n\}$. Put $\hat{\alpha}_i = e_i(\bar{z}_i - \bar{x}_i)$, for $i = 1, \ldots, n$. Then*

$$\mathcal{R}^2_{\boldsymbol{A},\boldsymbol{b}}(\bar{\boldsymbol{z}}) - T^2 \geq \sum_{i \in \mathrm{D}(\bar{\boldsymbol{r}},\bar{\boldsymbol{x}})} (\hat{\alpha}_i + \beta_i).$$

Proof. From Lemma 6, we have $\|\bar{\boldsymbol{x}} - \boldsymbol{x}^*\|_2^2 = \mathcal{R}^2_{\boldsymbol{A},\boldsymbol{b}}(\bar{\boldsymbol{x}})$. Applying Lemma 8, we find that

$$\mathcal{R}^2_{\boldsymbol{A},\boldsymbol{b}}(\bar{\boldsymbol{x}}) - T^2 = \mathcal{R}_{\boldsymbol{A},\boldsymbol{b}}(\bar{\boldsymbol{z}}) - \sum_{i=1}^n \hat{\alpha}_i - T^2 = \sum_{i \in \mathrm{D}(\bar{\boldsymbol{r}},\bar{\boldsymbol{x}})} \beta_i.$$

It is straightforward to check that $\hat{\alpha}_i \geq 0$ and $\sum_{i \in \{j : x_j = z_j\}} \hat{\alpha}_i = 0$. Hence we have

$$\begin{aligned}
\mathcal{R}^2_{\boldsymbol{A},\boldsymbol{b}}(\bar{\boldsymbol{z}}) - T^2 &= \sum_{i=1}^n \hat{\alpha}_i + \sum_{i \in \mathrm{D}(\bar{\boldsymbol{r}},\bar{\boldsymbol{x}})} \beta_i \\
&= \sum_{i \in \mathrm{D}(\bar{\boldsymbol{x}},\bar{\boldsymbol{z}}) \bigcup \mathrm{D}(\bar{\boldsymbol{r}},\bar{\boldsymbol{x}})} \hat{\alpha}_i + \sum_{i \in \mathrm{D}(\bar{\boldsymbol{r}},\bar{\boldsymbol{x}})} \beta_i \\
&\geq \sum_{i \in \mathrm{D}(\bar{\boldsymbol{r}},\bar{\boldsymbol{x}})} (\hat{\alpha}_i + \beta_i). \quad \square
\end{aligned}$$

Lemma 14. *Let $\bar{\boldsymbol{x}} \in \bar{S}_{\boldsymbol{A}}(\boldsymbol{b})$, $\bar{\boldsymbol{r}} \in \mathcal{T}$ and $\alpha_i = e_i(\bar{z}_i - |\bar{r}_i - 1|)$, for $i = 1, \ldots, n$. Then*

$$\mathcal{R}^2_{\boldsymbol{A},\boldsymbol{b}}(\bar{\boldsymbol{z}}) - T^2 \geq \sum_{i \in \mathrm{D}(\bar{\boldsymbol{r}},\bar{\boldsymbol{x}})} (\alpha_i + \beta_i).$$

Proof. By the definition of α,

$$\alpha_i = e_i(\bar{z}_i - |\bar{r}_i - 1|) = e_i(\bar{z}_i - \bar{x}_i) = \hat{\alpha}_i, \quad \text{for all } i \in \mathrm{D}(\bar{\boldsymbol{x}}, \bar{\boldsymbol{r}}). \tag{9}$$

From Lemma 13 and Eq. (9), we find that

$$\mathcal{R}^2_{\boldsymbol{A},\boldsymbol{b}}(\bar{\boldsymbol{z}}) - T^2 \geq \sum_{i \in \mathrm{D}(\bar{\boldsymbol{r}},\bar{\boldsymbol{x}})} (\hat{\alpha}_i + \beta_i) = \sum_{i \in \mathrm{D}(\bar{\boldsymbol{r}},\bar{\boldsymbol{x}})} (\alpha_i + \beta_i),$$

as desired. □

Let $\gamma_i = \alpha_i + \beta_i$ and ϕ be a permutation of $\{1, \ldots, n\}$ such that $\gamma_{\phi(1)} \leq \gamma_{\phi(2)} \leq \cdots \leq \gamma_{\phi(n)}$, which can be obtained by sorting the entries γ_i in increasing order.

Please cite this article in press as: W. Fortes, K.J. Batenburg, Quality bounds for binary tomography with arbitrary projection matrices, Discrete Applied Mathematics (2014), http://dx.doi.org/10.1016/j.dam.2014.01.026

Theorem 15. *Let* $\bar{\boldsymbol{x}} \in \bar{S}_{\boldsymbol{A}}(\boldsymbol{b})$ *and* $\bar{\boldsymbol{r}} \in \mathcal{T}$. *Define* $\alpha_i = e_i(\bar{z}_i - |\bar{r}_i - 1|)$ *and* $\gamma_i = \alpha_i + \beta_i$, *for* $i = 1, \ldots, n$. *Put*

$$U = \max\left\{0 \le \ell \le n : \sum_{i=1}^{\ell} \gamma_{\phi(i)} \le \mathcal{R}_{\boldsymbol{A},\boldsymbol{b}}(\bar{\boldsymbol{z}})^2 - T^2\right\}.$$

Then $\mathrm{d}(\bar{\boldsymbol{r}}, \bar{\boldsymbol{x}}) \le U$.

Proof. From Lemma 14 we have

$$\mathcal{R}^2_{\boldsymbol{A},\boldsymbol{b}}(\bar{\boldsymbol{z}}) - T^2 \ge \sum_{i \in \mathrm{D}(\bar{\boldsymbol{r}}, \bar{\boldsymbol{x}})} (\alpha_i + \beta_i) \ge \sum_{i=1}^{\mathrm{d}(\bar{\boldsymbol{r}}, \bar{\boldsymbol{x}})} \gamma_{\phi(i)},$$

which implies that $\mathrm{d}(\bar{\boldsymbol{r}}, \bar{\boldsymbol{x}}) \le U$. □

Theorem 15 is based on the following: consider the set of entries where $\bar{\boldsymbol{r}}$ and $\bar{\boldsymbol{x}}$ are different. If we transform $\bar{\boldsymbol{r}}$ into $\bar{\boldsymbol{x}}$ by performing a sequence of single-entry changes, each time an entry i of $\bar{\boldsymbol{r}}$ is changed the squared Euclidean distance from the current vector to $\boldsymbol{x}^*$ increases by $\beta_i = |2x_i^* - 1|$ and the current central radius reduces by $\alpha_i = e_i(\bar{z}_i - |\bar{r}_i - 1|)$.

Example 16. Using the same data given in Example 5, we compute $\mathcal{R}^2_{\boldsymbol{A},\boldsymbol{b}}(\bar{\boldsymbol{z}})$, the largest central radius that can be obtained by $\bar{\boldsymbol{z}} \in \{0, 1\}^n$, as given by Theorem 3.

$$\bar{\boldsymbol{z}} = \begin{pmatrix}1\\0\\1\\1\\1\end{pmatrix}, \quad \alpha = \begin{pmatrix}0.25\\0\\0\\0.25\\0\end{pmatrix}, \quad \gamma = \begin{pmatrix}0.5\\0.5\\0.75\\0.5\\0.75\end{pmatrix} \quad \text{and} \quad \gamma_\phi = \begin{pmatrix}0.5\\0.5\\0.5\\0.75\\0.75\end{pmatrix}.$$

With $\mathcal{R}^2_{\boldsymbol{A},\boldsymbol{b}}(\bar{\boldsymbol{z}}) - T^2 = 1.875 - 0.375 = 1.5$, we apply Theorem 15 and verify, for $0 \le \ell \le 5$, that

$$\sum_{i=0}^{3} \gamma_{\phi(i)} = 1.5 \le 1.5 \quad \text{and} \quad \sum_{i=0}^{4} \gamma_{\phi(i)} = 2.25 \not\le 1.5.$$

Then for any $\bar{\boldsymbol{x}} \in \bar{S}_{\boldsymbol{A}}(\boldsymbol{b})$, we have $\mathrm{d}(\bar{\boldsymbol{r}}, \bar{\boldsymbol{x}}) \le 3$.

Theorem 17. *Let* $\bar{\boldsymbol{x}}, \bar{\boldsymbol{y}} \in \bar{S}_{\boldsymbol{A}}(\boldsymbol{b})$ *and* $\bar{\boldsymbol{r}} \in \mathcal{T}$. *Define* $\alpha_i = e_i(\bar{z}_i - |\bar{r}_i - 1|)$ *and* $\gamma_i = \alpha_i + \beta_i$, *for* $i = 1, \ldots, n$. *Put*

$$U = \max\left\{0 \le \ell \le n : \sum_{i=1}^{\ell} \gamma_{\phi(i)} \le 2\left(\mathcal{R}^2_{\boldsymbol{A},\boldsymbol{b}}(\bar{\boldsymbol{z}}) - T^2\right)\right\}.$$

Then $\mathrm{d}(\bar{\boldsymbol{x}}, \bar{\boldsymbol{y}}) \le U$.

Proof. From Lemma 14 we have

$$2\left(\mathcal{R}^2_{\boldsymbol{A},\boldsymbol{b}}(\bar{\boldsymbol{z}}) - T^2\right) \ge \sum_{i \in \mathrm{D}(\bar{\boldsymbol{r}}, \bar{\boldsymbol{x}})} \gamma_i + \sum_{i \in \mathrm{D}(\bar{\boldsymbol{r}}, \bar{\boldsymbol{y}})} \gamma_i = \sum_{i \in \mathrm{D}(\bar{\boldsymbol{x}}, \bar{\boldsymbol{y}})} \gamma_i + \sum_{i \in \mathrm{D}(\bar{\boldsymbol{r}}, \bar{\boldsymbol{x}}) \bigcap \mathrm{D}(\bar{\boldsymbol{r}}, \bar{\boldsymbol{y}})} 2\gamma_i. \tag{10}$$

As $\gamma_i \ge 0$, for all $i = 1, \ldots, n$, then

$$2\left(\mathcal{R}^2_{\boldsymbol{A},\boldsymbol{b}}(\bar{\boldsymbol{z}}) - T^2\right) \ge \sum_{i \in \mathrm{D}(\bar{\boldsymbol{x}}, \bar{\boldsymbol{y}})} \gamma_i \ge \sum_{i=1}^{\mathrm{d}(\bar{\boldsymbol{x}}, \bar{\boldsymbol{y}})} \gamma_{\phi(i)}, \tag{11}$$

which implies that $\mathrm{d}(\bar{\boldsymbol{x}}, \bar{\boldsymbol{y}}) \le U$. □

7. Numerical experiments

A series of experiments was performed to investigate the practical value of the bounds given in the theorems and corollaries presented in the previous sections, where the bounds were evaluated for a range of problems. The experiments have been performed for two basic acquisition geometries: parallel beam and fan beam tomography. All experiments are based on simulated projection data obtained by computing the projection data from the test images (so-called *phantoms*) in Fig. 1. We refer to [5] for information on the origin of these phantoms.

All phantoms have a size of 512×512 pixels. To perform experiments for images with varying image size (smaller than 512×512), the phantoms have been downscaled to obtain binary images of the appropriate sizes.

The remainder of this section is structured as follows. Brief descriptions of parallel beam tomography and fan beam tomography are presented in Section 7.1. The quality of the bounds on the *length* of binary solutions is evaluated in Section 7.2. Experiments with bounds on the difference between binary solutions for the tomography problem are presented in Section 7.3.

Please cite this article in press as: W. Fortes, K.J. Batenburg, Quality bounds for binary tomography with arbitrary projection matrices, Discrete Applied Mathematics (2014), http://dx.doi.org/10.1016/j.dam.2014.01.026

(a) Phantom 1. (b) Phantom 2. (c) Phantom 3. (d) Phantom 4.

Fig. 1. Original phantom images used for the experiments.

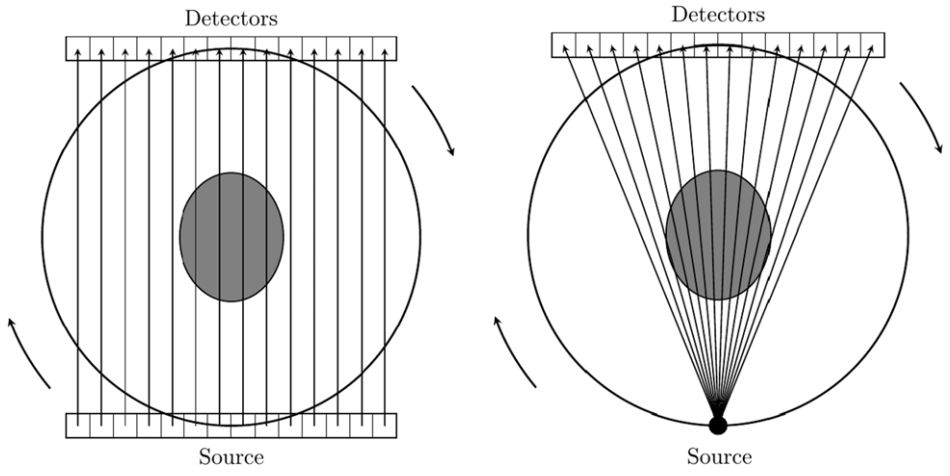

(a) Parallel beam geometry. (b) Fan beam geometry.

Fig. 2. Tomography geometry.

7.1. Tomography models

Throughout the tomography literature, several imaging models have been considered [13, section 7.4.1]. The unknown image is often approximated by an image defined on a discrete pixel grid. In *parallel beam tomography*, a projection is computed by considering a set of parallel rays in a given direction and computing a weighted sum of all the pixels that intersect with each ray, see Fig. 2(a). We select projection angles equally spaced between 0° and 180°.

In *fan beam tomography*, a point source emits a set of rays in all directions and an array of detectors measures the weighted sum of all the pixels that intersect with each ray, see Fig. 2(b). In our case, we assume that the detector is flat, i.e., all measurements are performed on a detector that follows a straight line. The phantom image is centered around the point of rotation of the source and detector. As the source and detector are positioned further away from the center of rotation, the fan beam geometry becomes more and more similar to a parallel beam geometry. We select projection angles equally spaced between 0° and 360°.

The intersection between a pixel and a ray can be computed in different ways, each leading to a different model for the imaging process. A common model for computing the projections of a pixelized image is the *line model*. In the line model, the weight a_{ij}, defined by the intersection between beam i and pixel j, is determined by the intersection length between the line (beam) and the pixel, Fig. 3(a).

In parallel beam tomography, for the case where the projection is aligned with the horizontal and vertical axes, the weight function of the line model has two discontinuities. Due to floating point errors, these can easily lead to pixel weights set to 0, where in fact they should be set to 1, or vice versa. The weighting scheme introduced by Joseph [12] does not have this drawback. Here, the weights a_{ij} are the interpolation coefficients obtained when tracing the line row by row (or column by column, depending on the projection angle), and applying linear interpolation between the centers of the two adjacent pixels, as shown in Fig. 3(b).

The *strip model* differs from the line model because the beam is a strip instead of a line. The weight a_{ij} is determined by the intersection area between strip i and the pixel j. For both line and Joseph's models, the column sums of their respective projection matrix is not constant while it is constant for the strip model in parallel beam tomography. Despite the fact that a projection matrix for the line model in parallel beam tomography does not have constant column sums, the variance of the

Please cite this article in press as: W. Fortes, K.J. Batenburg, Quality bounds for binary tomography with arbitrary projection matrices, Discrete Applied Mathematics (2014), http://dx.doi.org/10.1016/j.dam.2014.01.026

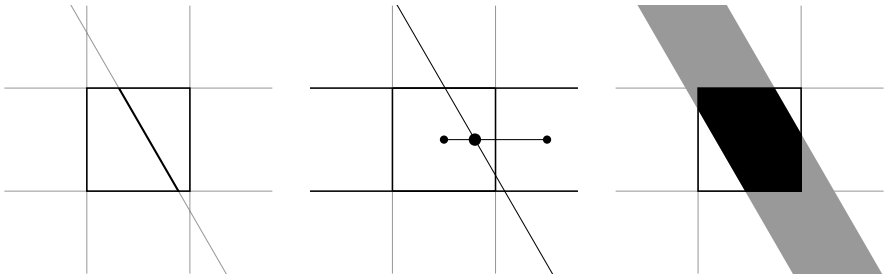

(a) Line model. (b) Joseph's model. (c) Strip model.

Fig. 3. Projection models.

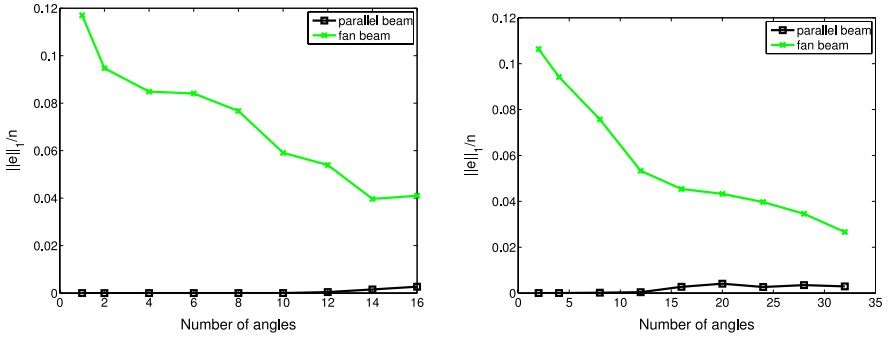

(a) Image size: 32 × 32. (b) Image size: 64 × 64.

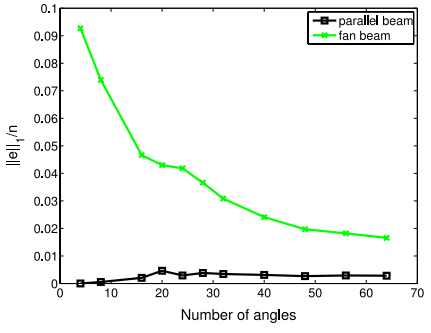

(c) Image size: 128 × 128.

Fig. 4. Relative ℓ_1-norm of the correction vector $\boldsymbol{e}$ for the line model in parallel and fan beam tomography.

column sums is small. The line model in fan beam tomography shows stronger difference as compared with the line model from parallel beam tomography. To show this, we have computed the *correction vector* $\boldsymbol{e}$ and plotted the sum of the absolute value of its entries divided by its number of entries using four projection angles, as shown in Fig. 4. Recall that when the projection matrix has constant column sums, the vector $\boldsymbol{e}$ is a null vector.

We will show experimental results for parallel beam tomography with the three projection models presented (line, Joseph's and strip). For fan beam tomography we use only the line model.

7.2. Bounds on the number of ones in binary solutions

The linear system (1) may have binary solutions with different lengths. In Section 4 we have presented different ways of computing an upper bound for the length of any binary solution. The expressions $D(1)$, $D(2)$ and $D(3)$ represent the difference between the computed upper bound for the number of ones of any binary solution (Theorems 1, 3 and 4, respectively) and the actual number of ones of the binary image used to construct the projections. A comparison between these bounds is shown in Fig. 5 for Phantom 4 with size 512 × 512. Fig. 5 includes three graphs, each one for a different parallel beam tomography model.

Please cite this article in press as: W. Fortes, K.J. Batenburg, Quality bounds for binary tomography with arbitrary projection matrices, Discrete Applied Mathematics (2014), http://dx.doi.org/10.1016/j.dam.2014.01.026

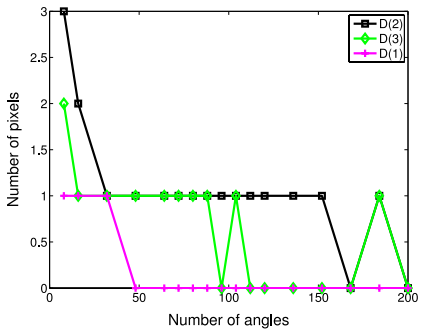

(a) Strip model.

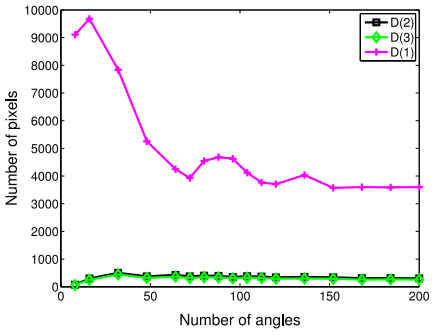

(b) Line model.

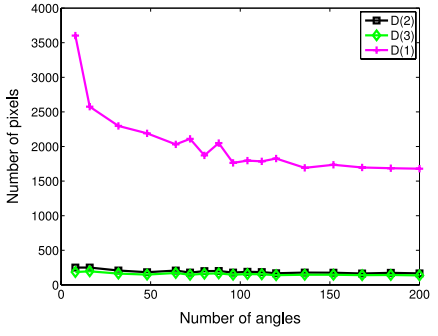

(c) Joseph's model.

Fig. 5. Absolute difference between the bound for the number of ones in any binary solution and the number of ones in the phantom.

The graph in Fig. 5(a) corresponds to the strip model, for which the projection matrix has the property of constant column sums except for numerical errors. Fig. 5(b) and (c) correspond to the line and Joseph's models.

It can be observed that for the strip model, the most basic bound is typically smaller than the other two, more refined, bounds. However, the number of pixels by which this bound differs from the other bounds is very small compared with the total number of pixels. The graphs for the line and Joseph's models show that the bound given in Theorem 1 can give very high bounds with a significant difference with respect to the other two bounds, which are close to each other. The bounds for the line and Joseph's model can be better visualized in Fig. 6. A comparison between these bounds is shown in Fig. 6 for Phantom 4 with size 512×512 for parallel beam tomography. Fig. 6 also includes the same bounds for Phantom 4 of size 128×128 with the line model for fan beam tomography.

The upper bound for the number of ones in binary solutions given in Theorem 4 is computed by the intersection of two functions. One of these functions is the linear function $g(\ell) = \ell$, which corresponds with the number of ones in a binary solution, while the other function is a concave function, which defines an upper bound on the number of ones. An example of a plot of these two functions can be seen in Fig. 7 for Phantom 4, using Joseph's model. The Phantom used for Fig. 7(a) has size 32×32 and 10 projection angles were used. For Fig. 7(b) the Phantom has size 128×128 with 32 projection angles. The results for fan beam tomography are somewhat similar to the ones of parallel beam tomography and are not shown here. Note that the graphs of the linear function g are almost vertical, due to the scale of the plots.

From Fig. 7(a), we have $300 < f(\ell) < 302$ for $0 \leq \ell < n$, so $\|\bar{\boldsymbol{x}}\|_1 = 301$. For the example in Fig. 7(b) the bound is not exact, but it is very close to the actual number of ones (4615) of the original phantom.

There is no guarantee that increasing the number of projection angles decreases the bound for the number of ones in the binary solutions. This implies that the bound for the number of ones can be recomputed every time a new angle is added and the smallest selected to generate the error bounds. This has not been done in the graphs of this article.

7.3. Bounds on the difference between binary solutions and binary approximate solutions

We now focus on the computation of the actual quality bounds for solutions of the binary reconstruction problem. A *binary approximate solution* is a binary vector that approximately satisfies the linear equation system $\boldsymbol{Ax} = \boldsymbol{b}$. In each experiment, the minimum norm solution $\boldsymbol{x}^*$ was first computed using the CGLS algorithm. For some bounds, it is necessary to compute the rounded central reconstruction $\bar{\boldsymbol{r}}$ which was performed by rounding $\boldsymbol{x}^*$ to the nearest binary vector, choosing $\bar{r}_i = 1$ if $x_i^* = \frac{1}{2}$. Based on $\bar{\boldsymbol{x}}$ and $\bar{\boldsymbol{r}}$, the various upper bounds described in Sections 3–6 were computed.

When presenting the results, we express the bounds on the pixel differences between two images as a *fraction* of the total number of image pixels. This allows for more straightforward interpretation of the results than using the absolute number

Please cite this article in press as: W. Fortes, K.J. Batenburg, Quality bounds for binary tomography with arbitrary projection matrices, Discrete Applied Mathematics (2014), http://dx.doi.org/10.1016/j.dam.2014.01.026

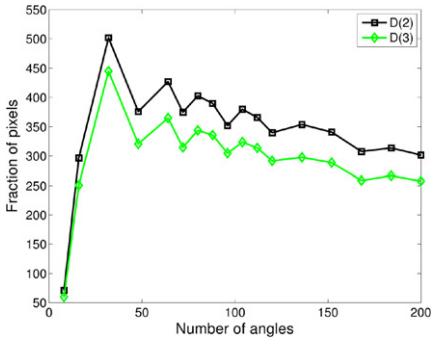

(a) Parallel beam: line model.

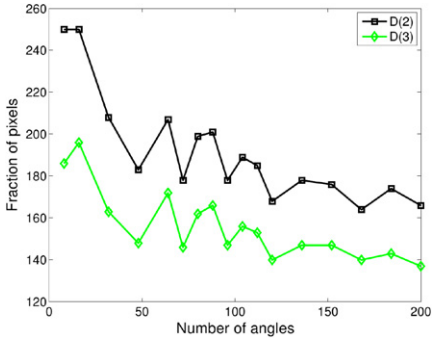

(b) Parallel beam: Joseph's model.

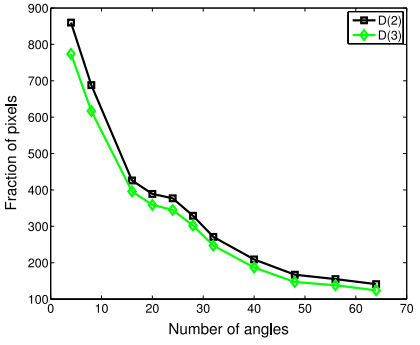

(c) Fan beam: line model.

Fig. 6. Absolute difference between the bound for the number of ones in any binary solution and the number of ones of the phantom.

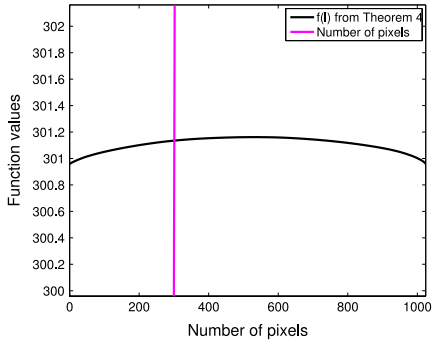

(a) Phantom 4 (32×32), 10 projections.

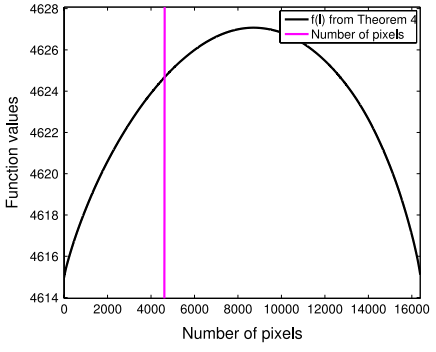

(b) Phantom 4 (128×128), 32 projections.

Fig. 7. Intersection between the two functions determines an upper bound for the length of any binary solution.

of pixel differences. As a substantial number of bounds will be given in a later part of this paper, we introduce the following notation:

- The expressions $U_d(1)$, $U_d(2)$ and $U_d(3)$ will represent bounds on the number of pixel differences between any two binary solutions of the reconstruction problem.
- The expressions $U_s(1)$ and $U_s(2)$ will represent bounds on the number of pixel differences between the *rounded central reconstruction* $\bar{\mathbf{r}}$ and any binary solution.

The bounds *within* each class U_d and U_s represent upper bounds for the same distance measure and can therefore be compared. The expression E_s denotes the number of pixel differences between the rounded central reconstruction and the phantom.

The expressions $U_d(1)$ is computed by using Theorem 7, $U_d(2)$ by using Theorem 11 and $U_d(3)$ by using Theorem 17. The expressions $U_s(1)$ and $U_s(2)$ are computed by using Theorems 9 and 15 respectively, which use the bound on the length of binary solutions from Theorem 4.

Please cite this article in press as: W. Fortes, K.J. Batenburg, Quality bounds for binary tomography with arbitrary projection matrices, Discrete Applied Mathematics (2014), http://dx.doi.org/10.1016/j.dam.2014.01.026

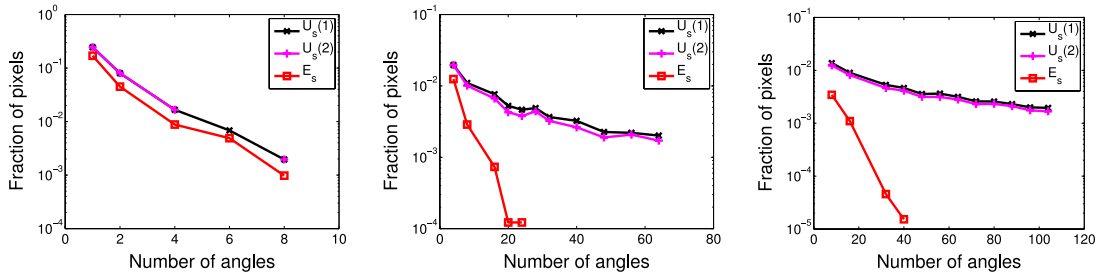

(a) Phantom 1, 32 × 32. (b) Phantom 1, 128 × 128. (c) Phantom 1, 256 × 256.

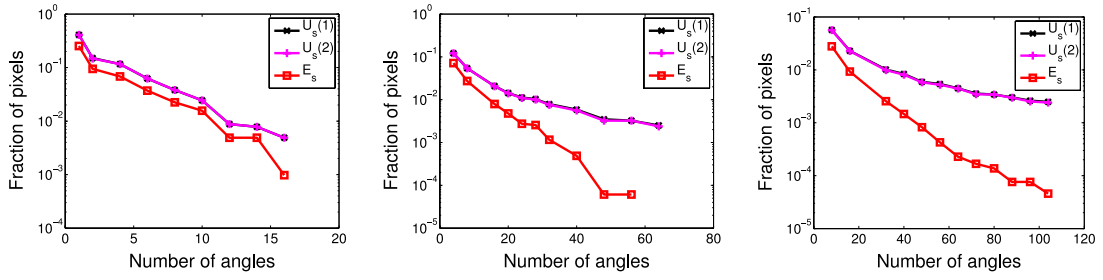

(d) Phantom 2, 32 × 32. (e) Phantom 2, 128 × 128. (f) Phantom 2, 256 × 256.

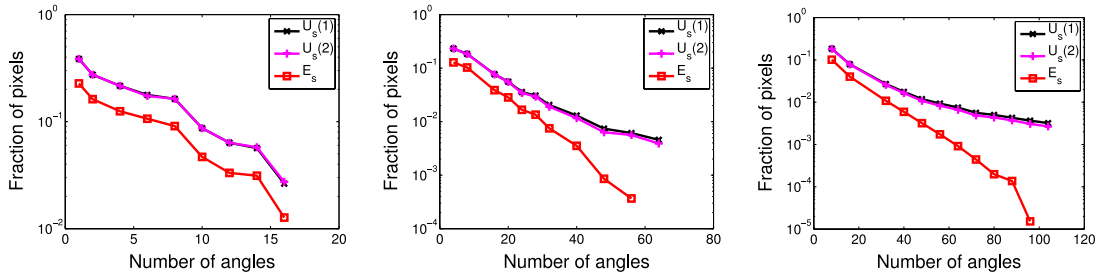

(g) Phantom 3, 32 × 32. (h) Phantom 3, 128 × 128. (i) Phantom 3, 256 × 256.

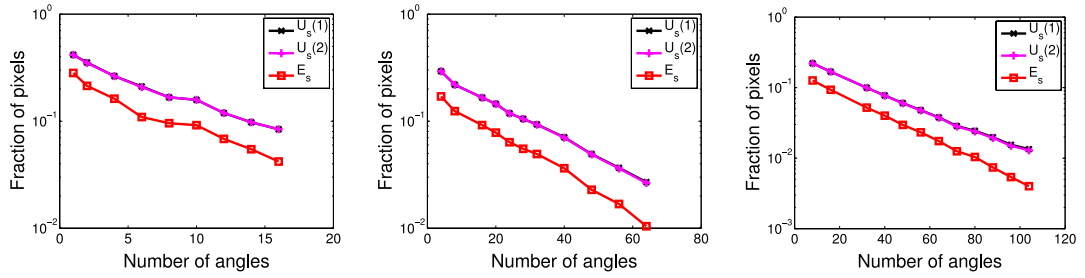

(j) Phantom 4, 32 × 32. (k) Phantom 4, 128 × 128. (l) Phantom 4, 256 × 256.

Fig. 8. Parallel beam, Joseph's model: computed U_s bounds as a function of the number of projection angles.

Several graphs presented in this section use a logarithmic scale for the error bounds. In some cases, the bound may become very small, or even 0, resulting in a point on the graph that cannot be plotted. These points are simply removed from the plot, causing the graph to be disconnected.

7.3.1. *Parallel beam tomography*

Experiments have been performed based on the four phantom images, scaled to sizes of 32×32, 128×128 and 256×256 respectively, varying the number of projection directions. The first set of results are shown in Fig. 8, where bounds $U_s(1)$ and $U_s(2)$ on the number of differences between $\bar{\boldsymbol{r}}$ and the phantom image $\bar{\boldsymbol{x}}$, and the exact error between $\bar{\boldsymbol{r}}$ and the phantom image $\bar{\boldsymbol{x}}$ are jointly plotted. In Fig. 9, the bounds $U_d(1)$, $U_d(2)$ and $U_d(3)$ on the distance between any two binary solutions

Please cite this article in press as: W. Fortes, K.J. Batenburg, Quality bounds for binary tomography with arbitrary projection matrices, Discrete Applied Mathematics (2014), http://dx.doi.org/10.1016/j.dam.2014.01.026

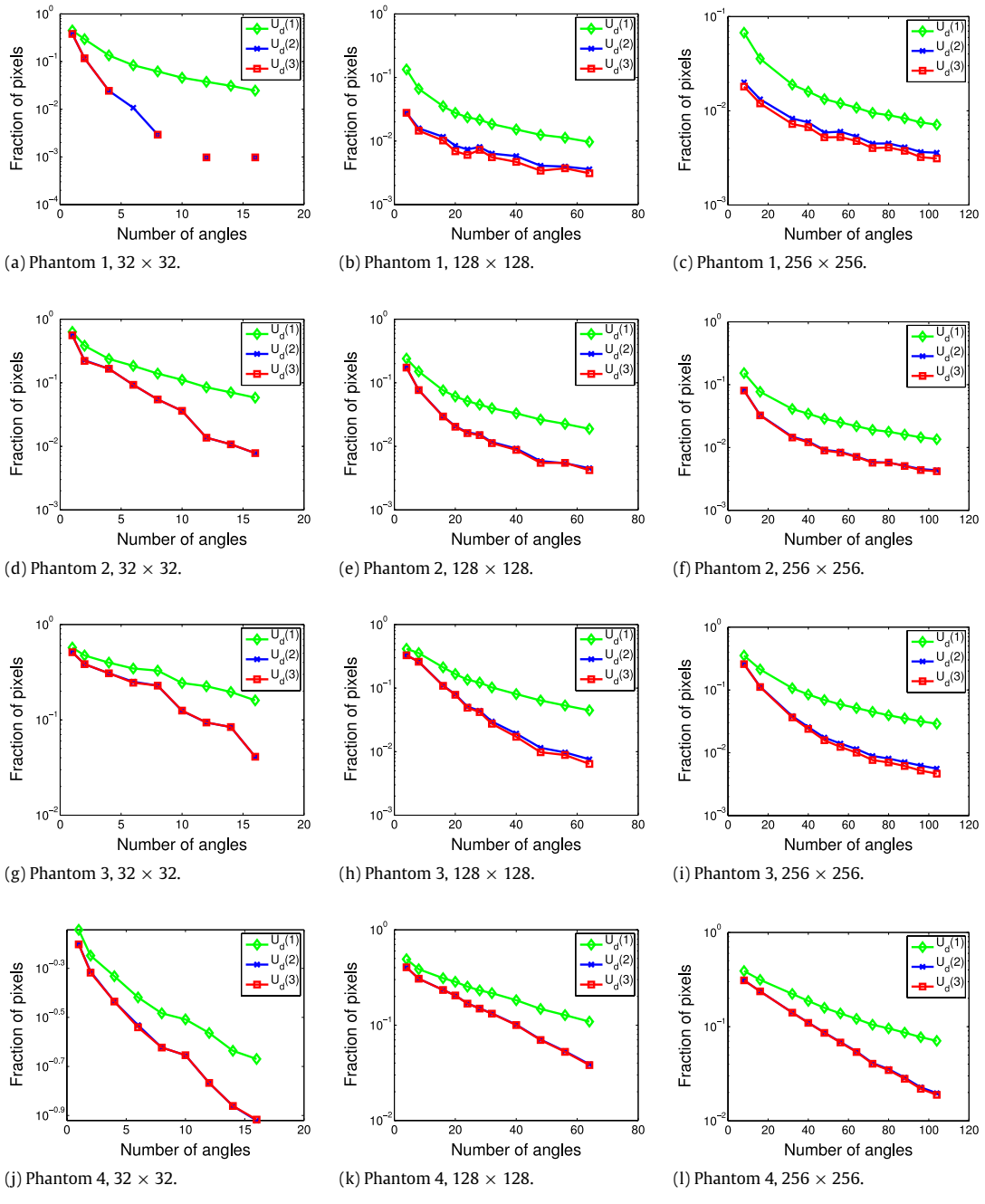

(a) Phantom 1, 32 × 32. (b) Phantom 1, 128 × 128. (c) Phantom 1, 256 × 256.

(d) Phantom 2, 32 × 32. (e) Phantom 2, 128 × 128. (f) Phantom 2, 256 × 256.

(g) Phantom 3, 32 × 32. (h) Phantom 3, 128 × 128. (i) Phantom 3, 256 × 256.

(j) Phantom 4, 32 × 32. (k) Phantom 4, 128 × 128. (l) Phantom 4, 256 × 256.

Fig. 9. Parallel beam, Joseph's model: computed U_d bounds as a function of the number of projection angles.

of the reconstruction problem are shown for the same experiments. For both Figs. 8 and 9 we used Joseph's model, which has results similar to the line model.

7.3.2. Fan beam tomography

Experiments have been performed based on the four phantom images, scaled to sizes of 32×32, 128×128 and 256×256 respectively, varying the number of projection directions. The first results are shown in Fig. 10, where bounds $U_s(1)$ and $U_s(2)$ on the number of differences between $\bar{\boldsymbol{r}}$ and the phantom image $\bar{\boldsymbol{x}}$, and the exact error between $\bar{\boldsymbol{r}}$ and the phantom image $\bar{\boldsymbol{x}}$ are jointly plotted. In Fig. 11, the bounds $U_d(1)$, $U_d(2)$ and $U_d(3)$ on the distance between any two binary solutions of the reconstruction problem are shown for the same experiments.

Please cite this article in press as: W. Fortes, K.J. Batenburg, Quality bounds for binary tomography with arbitrary projection matrices, Discrete Applied Mathematics (2014), http://dx.doi.org/10.1016/j.dam.2014.01.026

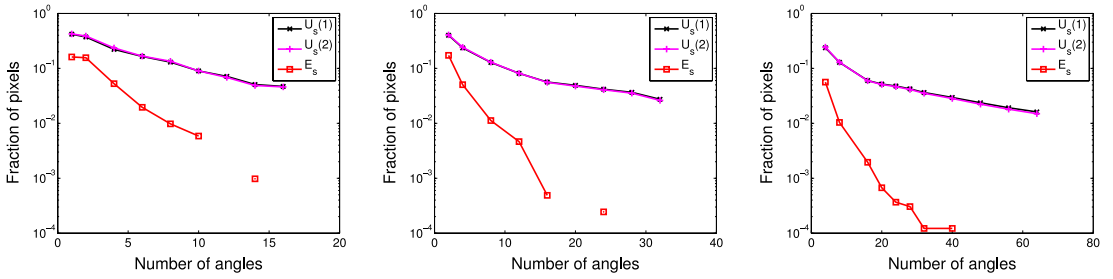

(a) Phantom 1, 32 × 32. (b) Phantom 1, 64 × 64. (c) Phantom 1, 128 × 128.

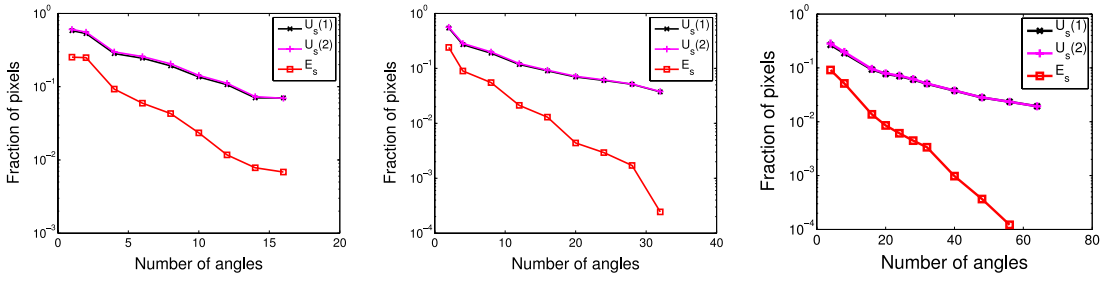

(d) Phantom 2, 32 × 32. (e) Phantom 2, 64 × 64. (f) Phantom 2, 128 × 128.

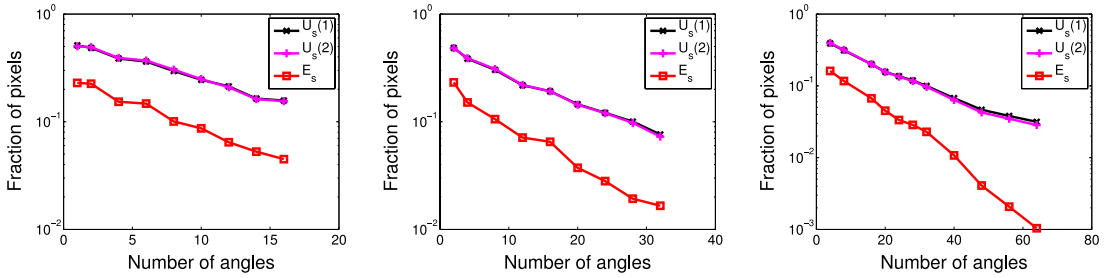

(g) Phantom 3, 32 × 32. (h) Phantom 3, 64 × 64. (i) Phantom 3, 128 × 128.

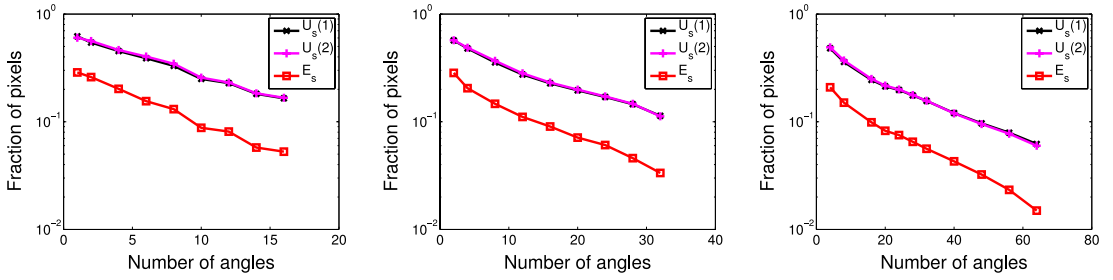

(j) Phantom 4, 32 × 32. (k) Phantom 4, 64 × 64. (l) Phantom 4, 128 × 128.

Fig. 10. Fan beam, line model: computed U_s bounds as a function of the number of projection angles.

7.4. Discussion of the results

Despite the facts that the four phantoms have strong differences in shape and morphology, and that the tomography models are quite different, the results shown in Figs. 8–11 are consistent throughout all experiments. In general, the bounds become smaller as the number of projection angles is increased.

From the difference between the bounds based on Section 4 and the bounds based on the rounded central reconstruction, we see that in most cases the phantom $\bar{\boldsymbol{x}}$ is substantially closer to $\bar{\boldsymbol{r}}$ than to $\boldsymbol{x}^*$.

In Figs. 8 and 10, it can be observed that the true fraction of pixel differences between the phantom image $\bar{\boldsymbol{x}}$ and the rounded central reconstruction $\bar{\boldsymbol{r}}$, denoted by E_s, is sometimes well approximated by the bound U_s, in particular for small

Please cite this article in press as: W. Fortes, K.J. Batenburg, Quality bounds for binary tomography with arbitrary projection matrices, Discrete Applied Mathematics (2014), http://dx.doi.org/10.1016/j.dam.2014.01.026

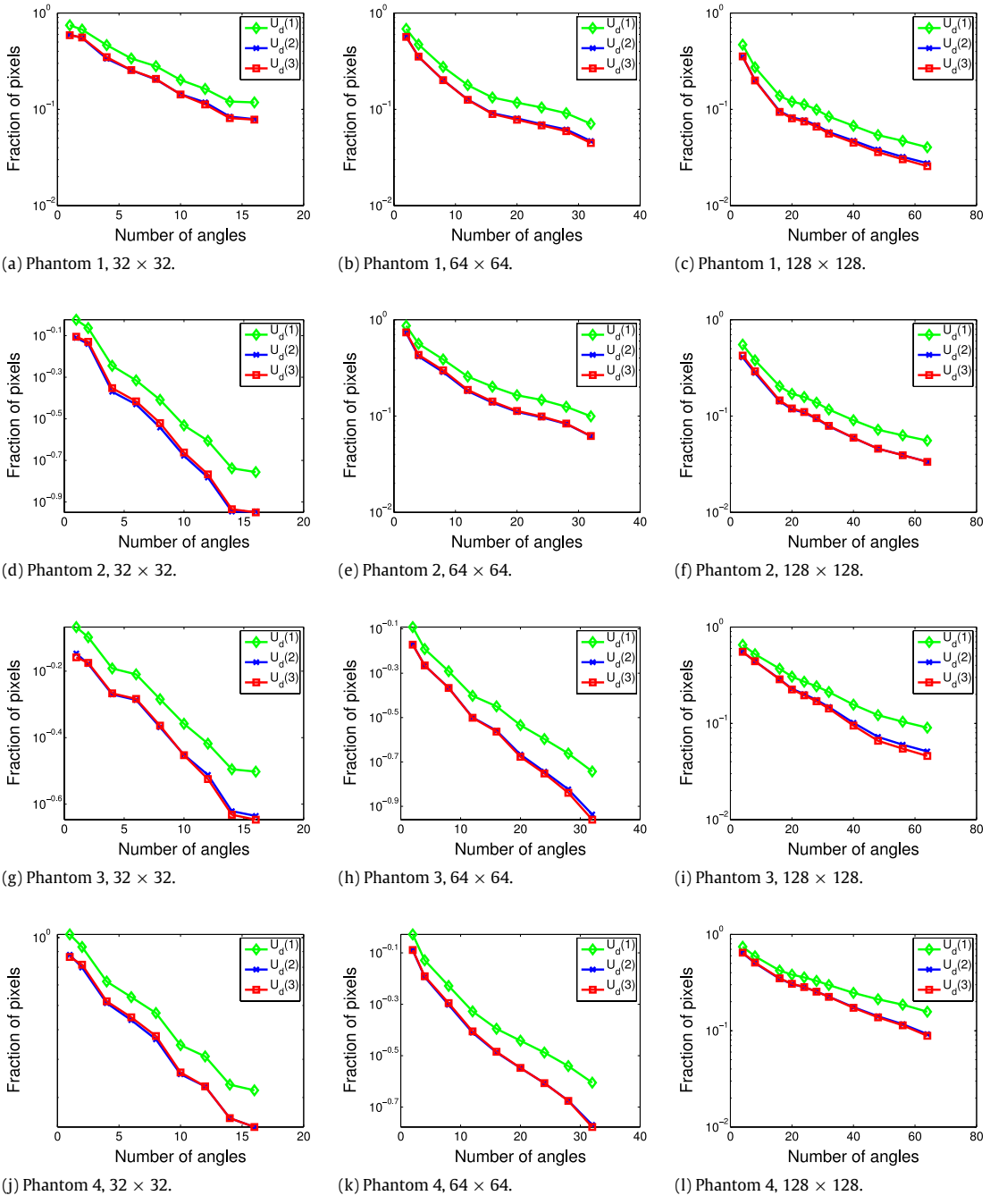

(a) Phantom 1, 32 × 32. (b) Phantom 1, 64 × 64. (c) Phantom 1, 128 × 128.

(d) Phantom 2, 32 × 32. (e) Phantom 2, 64 × 64. (f) Phantom 2, 128 × 128.

(g) Phantom 3, 32 × 32. (h) Phantom 3, 64 × 64. (i) Phantom 3, 128 × 128.

(j) Phantom 4, 32 × 32. (k) Phantom 4, 64 × 64. (l) Phantom 4, 128 × 128.

Fig. 11. Fan beam, line model: computed U_d bounds as a function of the number of projection angles.

images. Although bounding errors for the line model for fan beam tomography is more challenging than for parallel beam tomography, the bounds are reasonably low and effective.

In some of the figures, parts of the graph for $U_s(2)$ are missing, caused by zero values that cannot be displayed in the logarithmic scale. This can even occur due to numerical inaccuracies in the computation of the bounds if the true, correct bound is slightly larger than 0.

8. Outlook and conclusions

In this article, we have presented a range of general bounds on the accuracy of binary solutions, with respect to the unknown original vector. The bounds are based on an approach initiated in [5], where the authors presented bounds for the

Please cite this article in press as: W. Fortes, K.J. Batenburg, Quality bounds for binary tomography with arbitrary projection matrices, Discrete Applied Mathematics (2014), http://dx.doi.org/10.1016/j.dam.2014.01.026

case that the projection matrix has constant column sums. In the present paper, bounds have been derived that are much more general as they do not depend on this assumption.

Our bounds can be computed within reasonable time and give guarantees: (i) on the number of vector entries that can be different between any two binary solutions of an underdetermined problem and (ii) on the difference between a vector obtained by rounding the central reconstruction and any binary solution. The experimental results for parallel beam and fan beam tomography show that for certain sets of projection data the bounds computed by our method allow to prove that the number of differences between binary solutions of the reconstruction problem must be very small, even if the corresponding real-valued system of equations is severely underdetermined.

Acknowledgments

W.F. acknowledges support from the University of Leiden, The Netherlands. K.J.B. was supported by The Netherlands Organisation for Scientific Research (NWO), programme 639.072.005.

References

[1] A. Alpers, Instability and Stability in Discrete Tomography, Ph.D. Thesis, Technische Universität München, Shaker Verlag, ISBN 3-8322-2355-X, 2003.
[2] A. Alpers, S. Brunetti, Stability results for the reconstruction of binary pictures from two projections, Image Vis. Comput. 25 (2007) 1599–1608.
[3] A. Alpers, P. Gritzmann, On stability, error correction, and noise compensation in discrete tomography, SIAM J. Discrete Math. 20 (2006) 227–239.
[4] K.J. Batenburg, Analysis and optimization of an algorithm for discrete tomography, Electron. Notes Discrete Math. 12 (2003) 35–46.
[5] K.J. Batenburg, W. Fortes, L. Hajdu, R. Tijdeman, Bounds on the quality of reconstructed images in binary tomography, Discrete Appl. Math. 161 (15) (2013) 2236–2251.
[6] A. Ben-israel, T.N.E. Greville, Generalized Inverses: Theory and Applications, Canadian Math. Soc., 2002.
[7] Å. Björck, Numerical Methods for Least Square Problems, SIAM, Linköping University, Sweden, 1996.
[8] S. Brunetti, A. Daurat, Stability in discrete tomography: some positive results, Discrete Appl. Math. 147 (2005) 207–226.
[9] G.T. Herman, Fundamentals of Computerized Tomography: Image Reconstruction from Projections, Springer, 2009.
[10] G.T. Herman, A. Kuba (Eds.), Discrete Tomography: Foundations, Algorithms and Applications, Birkhäuser, Boston, 1999.
[11] G.T. Herman, A. Kuba (Eds.), Advances in Discrete Tomography and its Applications, Birkhäuser, Boston, 2007.
[12] P.M. Joseph, An improved algorithm for reprojecting rays through pixel images, IEEE Trans. Med. Imag. MI-1 (1982) 192–196.
[13] A.C. Kak, M. Slaney, Principles of Computerized Tomographic Imaging, SIAM, 2001.
[14] Y. Saad, Iterative Methods for Sparse Linear Systems, SIAM, Philadelphia, PA, USA, 2003.
[15] B. Van Dalen, On the difference between solutions of discrete tomography problems, J. Comb. Number Theory 1 (2009) 15–29.
[16] B. Van Dalen, On the difference between solutions of discrete tomography problems II, Pure Math. Appl. 20 (2009) 103–112.
[17] B. Van Dalen, Stability results for uniquely determined sets from two directions in discrete tomography, Discrete Math. 309 (2009) 3905–3916.
[18] B. Van Dalen, L. Hajdu, R. Tijdeman, Bounds for discrete tomography solutions, Indag. Math. 24 (2013) 391–402.
[19] G. Van Gompel, K.J. Batenburg, E. Van de Casteele, W. van Aarle, J. Sijbers, A discrete tomography approach for superresolution micro-ct images: application to bone, in: Proc. of IEEE International Symposium on Biomedical Imaging, 2010, pp. 816–819.
[20] G. Van Gompel, M. Defrise, K.J. Batenburg, Reconstruction of a uniform star-object from interior X-ray data: uniqueness, stability, and algorithm, Inverse Problems 25 (2009) 65010.

Please cite this article in press as: W. Fortes, K.J. Batenburg, Quality bounds for binary tomography with arbitrary projection matrices, Discrete Applied Mathematics (2014), http://dx.doi.org/10.1016/j.dam.2014.01.026